

The circumstellar material around SN IIn 1997eg: Another detection of Very Narrow P Cygni profile[★]

Isabel Salamanca¹, Roberto J. Terlevich² and Guillermo Tenorio-Tagle³

¹*Observatory of Leiden, Postbus 9513, NL-2300 RA Leiden, The Netherlands.*

²*Institute of Astronomy, Madingley Road, Cambridge CB3 0HA, U.K.*

³*Instituto Nacional de Astrofísica Óptica y Electrónica, AP 51, 72000 Puebla, México.*

Accepted ... Received ...; in original form 2000 December 16

ABSTRACT

We report the detection of a very narrow P Cygni profile on top of the broad emission $H\alpha$ and $H\beta$ lines of the Type IIn Supernova 1997eg. A similar feature has been detected in SN 1997ab (Salamanca et al. 1998), SN 1998S (Meikle & Geballe 1998, Fassia et al. 2001) and SN 1995G (Filippenko & Schlegel 1995). The detection of the narrow P Cygni profile indicates the existence of a dense circumstellar material (CSM) into which the ejecta of the supernova is expanding. From the analysis of the spectra of SN 1997eg we deduce (a) that such CSM is very dense ($n \gtrsim 5 \times 10^7 \text{ cm}^{-3}$), (b) that has a low expanding velocity of about 160 km s^{-1} . The origin of such dense CSM can be either a very dense progenitor wind ($\dot{M} \sim 10^{-2} M_{\odot} \text{ yr}^{-1}$) or a circumstellar shell product of the progenitor wind expanding into a high pressure environment.

Key words: circumstellar matter – ISM : individual : SN 1997eg – supernova remnants

1 INTRODUCTION

SN 1997eg is a Type IIn supernova discovered on 1997 December 5 (Nakano & Masakatsu 1997) having an unfiltered CCD magnitude of 15.6. Its coordinates are R.A. = $13^{\text{h}}11^{\text{m}}36^{\text{s}}.73$ and DEC = $+22^{\circ}55'29''.4$ (equinox 2000.0), which is $4''.1$ west and $33''.1$ north of the center of the host galaxy NGC 5012, a spiral galaxy with morphological type SAB(rs)c that host a low luminosity AGN in its center, and is situated at 50 Mpc (Ho, Filippenko, Sargent 1997). From the analysis of a spectrum taken 15 days later, Filippenko & Barth (1997) report that in the optical range, SN 1997eg show the typical features of Type IIn SN: absence of broad P Cygni profiles and, instead, strong emission lines, notably $H\alpha$ and $H\beta$ lines, on top of a very blue continuum - like most Type IIn supernovae. The He I 5876 Å is very strong, suggesting either a very high Helium abundance or a blend with the Na I 5894 Å blend. From the ratio of the [O III] 4363/5007 lines they deduce the presence of a very dense circumstellar material ($n \gtrsim 10^8 \text{ cm}^{-3}$). Besides, lines of very high excitation like He II 4886 Å or [Fe X] 6375 Å are prominent (Filippenko & Barth 1997) indicating the presence of

hard radiation. Finally, SN 1997eg has been detected in radio with the Very Large Array (VLA). The flux measured was $0.52 \pm 0.06 \text{ mJy}$ at 3.6 cm on 1998 May 31 and 0.53 ± 0.12 on 1998 June 9 (Lacey & Weiler 1998).

The exact date of explosion of SN 1997eg is not known, only that it was not seen on 1997 August 11 (~ 4 months before its discovery). We will adopt the discovery date as the date of explosion. Therefore, our data were taken when the supernova had an age of about 200 days.

2 THE OBSERVATIONS

On June 20 and July 16 1998, SN 1997eg was observed with the Utrecht Echelle spectrograph (UES) and ISIS respectively at the 4.2-m William Herschel Telescope (WHT) at “El Roque de los Muchachos” Observatory (La Palma, Spain). The echelle observations were done with a 2148×2148 SITE CCD and the 79.0 lines/mm grating. The long slit ones were done with a 1024×1024 Tek CCD and the R158R grating for the red arm of ISIS and with a 2148×4200 EEV CCD together with the grating R600B for the blue arm. The observing log is given in Table 1. The data were calibrated using the standard procedures within IRAF: they were debiased, trimmed, flat-fielded using a normalized flat field, and calibrated in wavelength by using arc lamps of Th-Ar for the echelle spectra and Ne-Ar for the long slit

[★] Based on observations made with the 4.2-m William Herschel Telescope, operated on the island of La Palma by the Isaac Newton Group in the Spanish Observatorio del Roque de los Muchachos of the Instituto de Astrofísica de Canarias.

ones. Flux calibration was performed by using the standard stars BD+33 2642 and BD+26 2606 respectively. The atmospheric extinction was applied using the mean extinction curve for La Palma. Finally, the spectra were corrected by redshift, thus all the wavelengths cited here are at rest frame.

3 ANALYSIS

3.1 Redshift and distance of SN 1997eg

The redshift, and therefore the heliocentric radial velocity and distance to SN 1997eg can be determined from the narrow lines. We take the echelle spectra because of its higher spectral resolution. We choose the narrow lines [Fe XIV] 5303 Å, [N II] 5755 Å and [Fe X] 6375 Å. These are among the lines with better signal-to-noise ratio in the echelle spectra and that are clearly associated with the circumstellar material of SN 1997eg (see section 3.5 and Fig. 7). The line [Fe XI] 7892 Å was discarded because of its double peak (see Fig. 3). The average redshift is 0.00837 ± 0.00004 , equivalent to $2511 \pm 12 \text{ km s}^{-1}$. The heliocentric velocity is therefore $2485 \pm 12 \text{ km s}^{-1}$. If we adopt a Hubble constant of $H_0 = 50 \text{ km s}^{-1} \text{ Mpc}^{-1}$ then the distance to SN 1997eg is 50 Mpc. Since the emission line in a P Cygni profile is partially absorbed it is difficult to position exactly the center of the profile. However, after having corrected the echelle spectra by redshift, the center of the H α P Cygni is at $\sim 6562.9 \text{ Å}$.

3.2 Contamination by the host galaxy

The extended H α and H β emission of the host galaxy, NGC 5012, is clearly visible on the 2D images of SN 1997eg. We have checked how much of the narrow P Cygni profile can be due to an effect of background subtraction. For that purpose we have extracted the echelle spectrum with and without background subtraction, and we have compared both results. In Fig. 1 we can see that the H α P Cygni in both spectra - with and without background subtraction - is almost equal. Therefore the extended H α emission does not play a significant role in the P Cygni profile.

3.3 Line identification

The most prominent lines are the Balmer series, H δ , H γ , H β and H α (see Fig. 2) together with Fe II emission. Other lines detected in the long slit spectra are the Oxygen lines, [O III] 4363 Å and [O III] 5007 Å, the lines of Helium He I 5876 Å and He I 7065 Å, and the blue side of the infrared Ca II triplet at $\sim 8500 \text{ Å}$. In addition, we identify in the echelle spectra several high excitation iron lines: [Fe XIV] 5303 Å, [Fe X] 6375 Å and [Fe XI] 7892 Å (see Fig. 3) as well as several low excitation lines of Fe II, [Fe II] and [Fe III]. In Table 2 we give a list of the emission lines identified in both, the long slit and echelle spectra. The Full Width at Half Maximum (FWHM) of the narrow lines is the one measured on the echelle spectra whenever possible, and it has been corrected by the instrumental resolution.

Finally, we must as well draw the attention to those lines that are *not* detected, like [N II] 6583 Å, [O I] 6300, 6364 Å

or the coronal lines [Ar X] 5533 Å, [Ca V] 5309 Å and [Fe XI] 7889 Å[†].

3.4 Balmer lines profiles

We show in Fig. 4 the profile of the four strongest Balmer lines, H α , H β , H δ and H γ . The continuum has been fitted and subtracted using a straight line and the maximum amplitude of the line has been set to one. For each line, the zero velocity corresponds to its rest-frame wavelength. Note that this corresponds to the central part of the narrow P Cygni profile. All the Full Width at Half Maximum (FWHM) given in this section have been corrected by instrumental response.

The most evident characteristic of the broad Balmer lines is that their profiles are asymmetric and flat topped.

The H α line seems composed of a central core and broad wings and has the red wing less extended than the blue wing. This is probably due to self-absorption. The FWHM is $\sim 3800 \text{ km s}^{-1}$ and The Full Width at 10% intensity is $\sim 11000 \text{ km s}^{-1}$. H α has also a very extended and weak blue wing extending up to $\sim 23000 \text{ km s}^{-1}$ (see Fig. 5). A similar extended blue wing was detected in SN 1997ab in the early spectra. In fact, overall, the H α profile in both supernovas, SN 1997ab and SN 1997eg, is remarkably similar, despite the probable difference of about 200 days in their age. The narrow P Cygni absorption is also detected in the long slit spectrum but not resolved.

The H β line is also asymmetric, and the red wing less extended than the blue one. However this effect is less pronounced than in H α . The FWHM of H β is $\sim 3200 \text{ km s}^{-1}$. Unfortunately, the red wing of H β is blended with Fe II emission, and nothing can be said about the extension of the wings. The core appears as flat-topped, and the narrow P Cygni line is detected, although it is not resolved in the low dispersion data.

The next Balmer line, H γ , has a core of about 3500 km s^{-1} FWHM, and is clearly flat-topped. The absorption component of the narrow P Cygni is detected, but the emission (if any) is lost in the noise. The H δ line is also present, although weaker and consequently with lower signal-to-noise ratio. Nevertheless, the absorption component of the narrow P Cygni is detected. The core of the broad line has a FWHM $\sim 2400 \text{ km s}^{-1}$. Contrary to H α and H β , the red side is more extended. The extension of the wings in these two lines is difficult to determine, because they are blended with Fe II emission.

In the high dispersion echelle spectra, we see that effectively both H α and H β lines are flat-topped (the rest of the Balmer series are outside the wavelength coverage of the echelle data). We can also see that the narrow, unresolved component becomes a clear P Cygni profile. The absorption component seems to be somewhat broader than the emission part. From the blue wing of the absorption we deduce that the material emitting such a profile is expanding at 160 km s^{-1} (see Fig. 6).

[†] The coronal line [Fe VII] 6087 Å falls in between two orders of the echelle spectra and therefore nothing can be said about its detection.

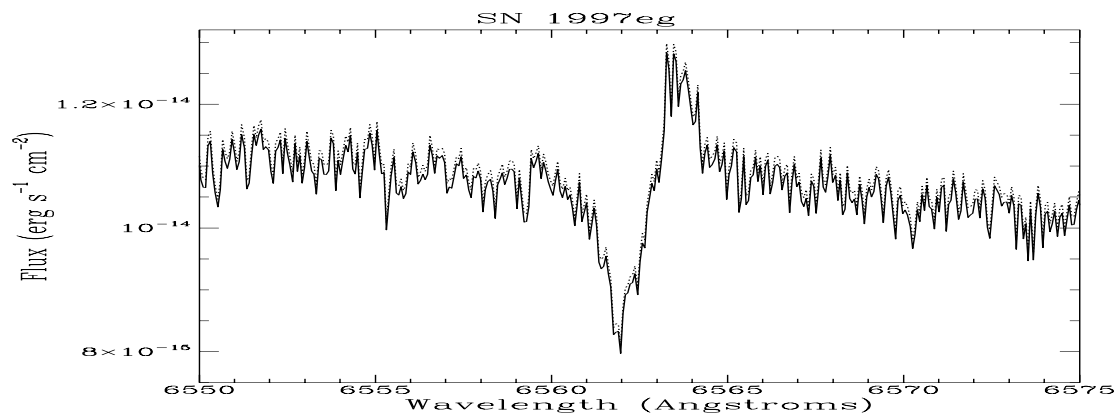


Figure 1. The narrow P Cygni is not affected by the galaxy subtraction, due to the extended H α and H β emission. In this figure we show two spectra, one extracted with background subtraction (solid line) and the other with no background subtraction (dotted line). As we can see there is practically no difference among them.

Table 1. Log of spectroscopic observations of SN 1997eg. The “+day” is the number of days elapsed since explosion (1997 December 5).

Date	age (days)	Instrument	Slit (arcsec)	Spect. range (Å)	Spect. resol. ^a (Å / km s ⁻¹)
20 June	+198	UES	1.2	4400 - 8977	0.10 - 0.19 / 6.5 km s ⁻¹
16 July	+224	ISIS Blue arm	2.0	3700 - 5480	3 / 185 km s ⁻¹
16 July	+224	ISIS Red arm	2.0	5550 - 8500	11.8 / 540 km s ⁻¹

^a As measured from the FWHM of the arc lines

3.5 The narrow lines

Another important observational characteristic on SN 1997eg is the presence of very narrow lines (FWHM between ~ 7 and 40 km s^{-1}) with a wide range of ionization potentials up to 360 eV. The most prominent ones are shown in Fig. 3. This wide range of ionization energies implies the existence of an ionizing continuum that extends at least between these values. In other words, SN 1997eg must be producing soft X rays.

If we plot the ionization potential (IP) of each narrow line versus its FWHM (Fig. 7) then it becomes clear that there are two different groups of lines. One set, with low IP (between 0 and 40 eV) and small FWHM (between 6 and 14 km s^{-1}). The other group has a much broader range of IP (between 8 and 361 eV), and a larger FWHM (between 25 and 40 km s^{-1}). This second group is probably related to the dense CSM that is surrounding the supernova, while the first may be related to the H II region where SN 1997eg exploded.

Finally, we must draw the attention to the fact that there are no broad forbidden lines.

4 INTERPRETATION: A DENSE CIRCUMSTELLAR MATERIAL

Type II_n Supernovae are associated with strong radiative shocks produced by the interaction of the fast SN ejecta with a dense circumstellar material (Shull 1980, Wheeler,

Mazurek, Sivaramakrishnan 1980, Chugai 1991, Chevalier & Fransson 1994, Terlevich et al. 1992, 1995). When a supernova explosion occurs, two shocks are produced: the leading shock ($v_{shock} \sim 10^4 \text{ km s}^{-1}$), that encounters and heats the CSM up to a temperature of $\sim 10^9 \text{ K}$, and the reverse shock ($v_{shock} \sim 10^3 \text{ km s}^{-1}$), that decelerates and thermalizes the ejecta to temperatures of about 10^7 K . In the standard case, when the SN explosion occurs in a medium of density $\sim 1 \text{ cm}^{-3}$, both shocks are adiabatic, and remain so for thousands of years. However, for very high densities ($n \gtrsim 10^7 \text{ cm}^{-3}$) the adiabatic phase is almost nonexistent, and the shocks become radiative a few months after the explosion, when the ejecta is still moving at high speeds (several times 1000 km s^{-1}), and when the size of the remnant is less than 0.01 pc (hence the name of “compact SN remnants” given by Terlevich et al. 1992, 1995). When this happens, we have the phenomena called “catastrophic cooling”, which means that the time scale for cooling is much lower than the time scale for pressure adjustment. In other words, there is a fraction of the shocked gas that cools and loses pressure too rapidly for the gas to adjust, and this generates secondary shocks that compresses the gas into two thin shells (one for each shock front, leading and forward). These thin layers have a density of $\sim 10^{9-13} \text{ cm}^{-3}$, a temperature of $\sim 10^4 \text{ K}$ and a velocity of few $\times 1000 \text{ km s}^{-1}$ (Terlevich et al. 1992).

Theoretical calculations show that if the CSM has a constant density, both the leading and reverse shocks become radiative (see Terlevich et al. 1992, 1995). However, if the density of the surrounding media decreases as r^{-2} as

Table 2. List of emission lines seen in the spectra of SN 1997eg. The first column is the observed (redshifted) wavelength in Angstroms. The second column is the line identification, the third is the full width at half maximum (corrected by the instrumental response) the fourth is the flux in units of 10^{-16} erg s $^{-1}$ cm $^{-2}$, the fifth indicates if the line is seen in the echelle spectra (UES) or the long-lsit one (ISIS), and the last column is the Ionisation Potential of the line.

Wavelength Å	Identification	FWHM km s $^{-1}$	Flux erg s $^{-1}$ cm $^{-2}$	Spectrum	Ion. Potential eV
3868.3	[Ne III] 3868.7	unresolved	5.0	ISIS	40
~4107	H δ	~2390	76	ISIS	13.6
~4343	H γ	~3510	~200	ISIS ^a	13.6
4339.2	H γ	unresolved	~-2.2	ISIS ^b	13.6
4363.4	[O III] 4363.2	unresolved	5.3	ISIS	35.1
4486.43	[Fe II] 4486.23	~35	7	UES	7.9
4609.04		26	7.8	UES	-
4658.26	Fe II 4658.0 or [Fe III] 4658.1	8	1.5	UES	7.9 or 16.18
4739.50	Mg II 4739.6	unresolved	1.6	UES	7.6
4838.69	4838.7	unresolved	0.9	UES ^c	-
4861.6	H β	3200 (core)	880	ISIS & UES ^d	13.6
4860.81	H β	40	-5.9	UES & ISIS	13.6
4861.86	H β	36	3.2	UES & ISIS	13.6
4899.72	4899.6	unresolved	2.8	UES ^c	-
4906.29	Fe IV 4906.2	unresolved	2.2	UES	30.65
4958.80	[O III] 4958.9	~30	2.0	UES ^e	35.1
4977.84	4977.6	~23	1.5	UES ^c	-
4988.36		unresolved	0.5	UES	-
5006.81	[O III] 5006.8	~40	3.8	ISIS & UES ^f	35.1
5040.99	Si II 5041.1	unresolved	0.7 + 0.9	UES	8.15
5077.16	[Fe II] 5076.6	unresolved	0.6	UES	7.9
5159.60	[Fe II] 5158.8	~6.5 ^g	0.8	UES	7.9
5176.03	N II 5175.9	~6.5 ^g	0.9	UES	14.5
5270.59	[Fe III] 5270.4	~25	1.3	UES	16.18
5302.78	[Fe XIV] 5302.9	~38	2.0	UES ^h	361.0
5429.18	[Fe VI] 5428.6 or Fe I 5429.7	14	0.8	UES	75.5 or 0
5438.97		30	0.8	UES	-
5440.18	[Fe II] 5440.5	unresolved	0.3	UES	7.9
5525.72	Fe II 5525.1	36+unresolv.	2.0	UES	7.9
5580.59	[Fe II] 5580.8	8	0.9	UES	7.9
5700.96		14	1.0	UES	-
5754.65	[N II] 5754.8	~34	9.4	UES & ISIS	14.5
5843.5		400	18	ISIS	-
~5875	He I 5876	7500	670	ISIS	24.6
5875.62	He I 5875.6	~10 + 30-40	-	UES	24.6
5875.98	He I 5876.0	-	2.3 (+)	UES ⁱ	24.6
5949.15		11	1.1	UES	-
6374.48	[Fe X] 6374.5	42	7.6	UES ^h	235.0
6506.15		unresolved	0.8	UES	-
~6551.2	H α	3800	9077	ISIS & UES ^j	13.6
6561.96	H α	53	-36.4	UES & ISIS ^b	13.6
~6563.5	H α	40	14.0	UES ^k	13.6
7065.5	He I 7065	~2750 + ~6000	24.6	ISIS ^l	24.6
7468.33	N I 7468.3	12	2.5	UES	0
7891.98	[Fe XI] 7891.9	31	3.3	UES ^h	262.1

^aFlat topped

^bThe narrow absorption of the P Cygni profile

^cSeen on symbiotic stars

^dFlat topped

^eVery noisy

^fUES marginal

^gJust resolved

^hCoronal line

ⁱThis line and the previous are not totally separated

^jThe strongest line

^kNarrow emission peak not well defined

^lBroad component blue-shifted

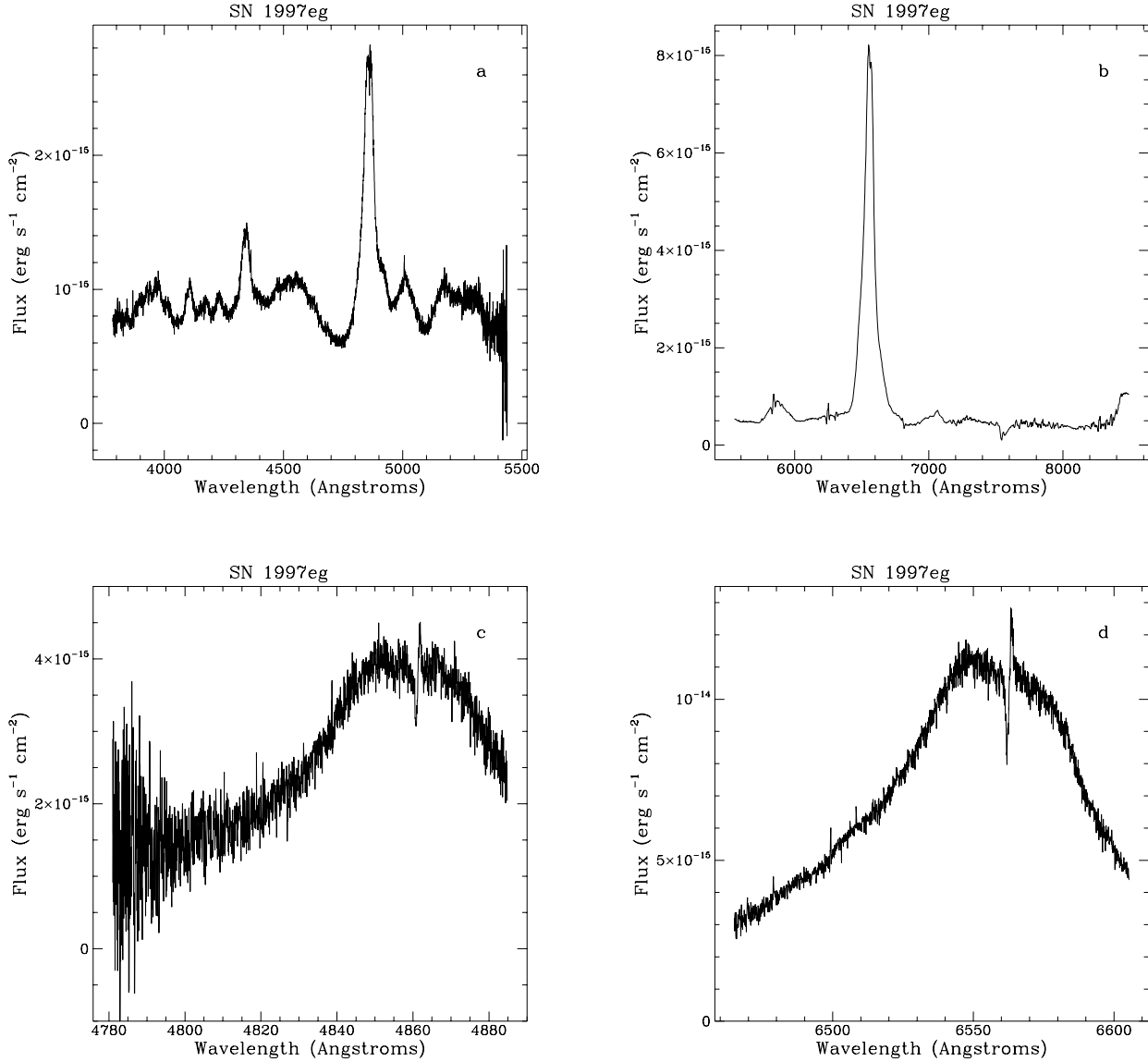


Figure 2. Spectra of SN1997eg. On the top panels, the long slit spectra taken with ISIS, (a) $H\beta$ and (b) $H\alpha$, and on the bottom the echelle spectra (only the order with $H\beta$ (c) and $H\alpha$ (d) are shown). The flux is in units of $\text{erg s}^{-1} \text{cm}^{-2}$ and the wavelength is in Angstroms.

is expected from a wind, the leading shock may stay adiabatic, and only the less luminous reverse shock becomes radiative (Chevalier & Fransson 1994). In any case, when either both or one shock becomes radiative, they will emit copious amounts of UV and X-ray photons which will ionize the freely expanding ejecta, the dense and fast thin shell and the surrounding CSM. The CSM is heated to a temperature of $\sim 10^{6-7}$ K to decay in a few months to $\sim 10^{5-6}$ K.

The thin shell and the free expanding ejecta are responsible for the broad lines, such as $H\alpha$ and $H\beta$, as well as for the blue continuum. On the other hand, the narrow emission lines (including the P Cygni) are emitted in the dense circumstellar material. Therefore, we can distinguish two main emitting regions: the circumstellar medium around SN 1997eg and the shocked material. The evolution of the

latter is dependent on the physical conditions of the first, mainly its density.

The fact that the broad $H\alpha$ and $H\beta$ lines are flat-topped confirms that they are emitted in an expanding thin shell. On the other hand, the presence of the narrow P Cygni profile proves the existence of a slowly expanding, dense material into which the ejecta of the supernova is expanding. Further observational evidence for the existence of such dense material comes from Fig. 7. There is a group of lines which have similar FWHM (between 30 and 40 km s^{-1}) but quite large range of IP. All the forbidden lines in this group have large critical densities ($\gtrsim 10^5 \text{ cm}^{-3}$).

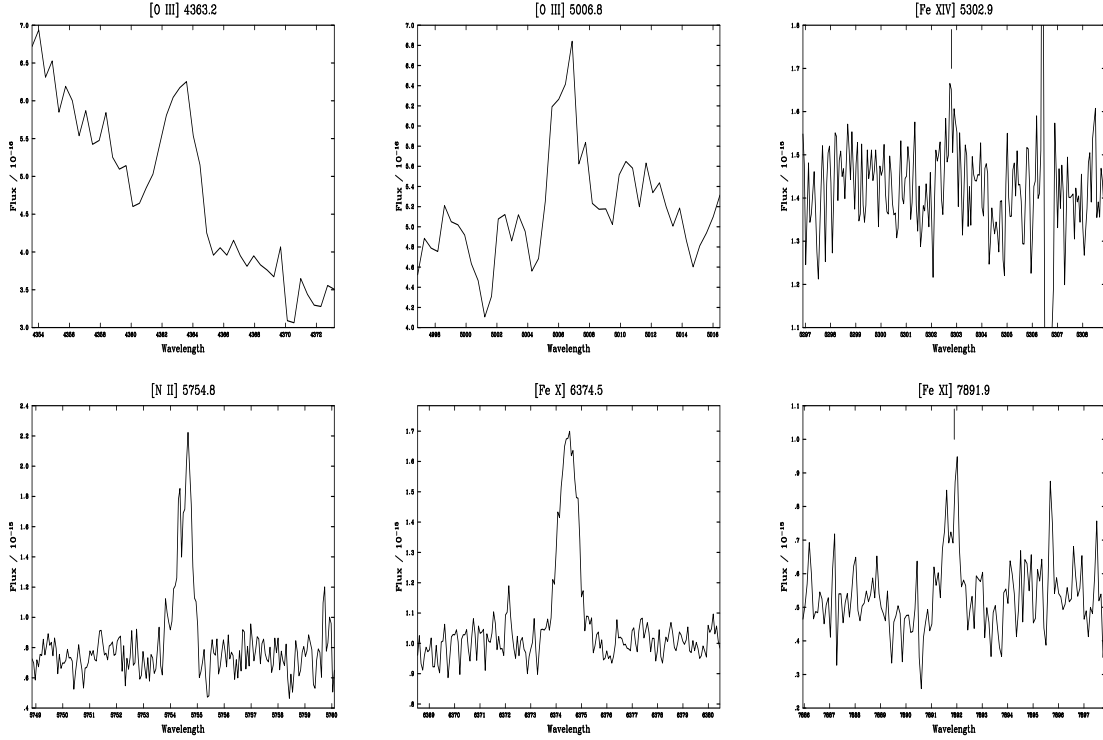


Figure 3. The most prominent narrow lines that are seen in the echelle spectra, ordered by increasing wavelength. The wavelength range is 12 Å except for [O III] 4363 Å and [O III] 5007 Å which is 20 Å.

4.1 Observed parameters

The following physical parameters can be deduced from the observations:

The luminosity of the broad Balmer lines:

$$L_{H\alpha}^B = 2.8 \times 10^{41} \text{ erg s}^{-1}$$

$$L_{H\beta}^B = 4.5 \times 10^{40} \text{ erg s}^{-1}$$

These values have been estimated in the low dispersion spectra, for an adopted distance of 50 Mpc.

Velocity of the gas emitting the broad Balmer lines:

$$v_s = 7000 \text{ km s}^{-1}$$

The freely expanding ejecta, the two thin shells associated with the backward and leading shocks, they all contribute to the flux of the broad Balmer lines. The maximum velocities are those of the ejecta, thus the flux in the extended wings of the Balmer lines will come mainly from there. Since there is probably some self-absorption, we only see the side that is moving towards us, i.e. the blue wing. The main contribution to the flux of the Balmer lines is coming from the thin shell associated with the leading shock. Its velocity can be determined therefore from the FWZI of the core of the Balmer lines. However, as said before, due to the self-absorption, we do not receive all of the flux emitted on the side receding from us. Therefore, the best is to measure the velocity at zero intensity of the bluest part of the core of the Balmer lines. The best for that purpose is $H\beta$ because, while having a good signal-to-noise ratio, it does not have the very broad and weak tail that is present in $H\alpha$ (see section 3.4). We must emphasize that this value is rather qualitative. In order to have more exact figures, one would need a more

detailed modelisation - which is beyond the scope of this paper.

The luminosity in the emission component of the narrow Balmer lines:

$$L_{H\alpha}^N = 4.0 \times 10^{38} \text{ erg s}^{-1}$$

$$L_{H\beta}^N = 1.1 \times 10^{38} \text{ erg s}^{-1}$$

These values are measured from the echelle spectra. In fact, the true values must be certainly larger since the blue side of the line is in absorption. To account for this and possible obscuration effects we have multiplied the observed emission luminosities by a factor 2. The $H\alpha$ line is more intense and has better signal-to-noise ratio, but it may be collisionally enhanced. The $H\beta$ line is not affected by collisional effects but it is affected by reddening, and is weaker, which means that its measured flux is more uncertain.

Velocity of the CSM:

$$v_w = 160 \text{ km s}^{-1}$$

It is measured from the blue wing of the absorption line in the P Cygni profile, in both $H\alpha$ and $H\beta$ (see Fig. 6). This value is larger than the velocity of 90 km s^{-1} obtained for SN 1997ab (Salamanca et al. 1998).

Temperature of the CSM:

The coronal lines [Fe X] 6374 Å, [Fe XI] 7892 Å and [Fe XIV] 5303 Å indicate a medium with a high temperature, $\sim 10^6$ K. On the other hand, the lines [O III] 4959, 5007 Å, [N II] 5755 Å, $H\beta$ or $H\alpha$ are formed in a somewhat cooler material, $\lesssim \text{few} \times 10^5$ K.

Density of the CSM:

We can impose constraints on its the density based on the ratio of the narrow lines, [O III] 5007 and [O III] 4363. For

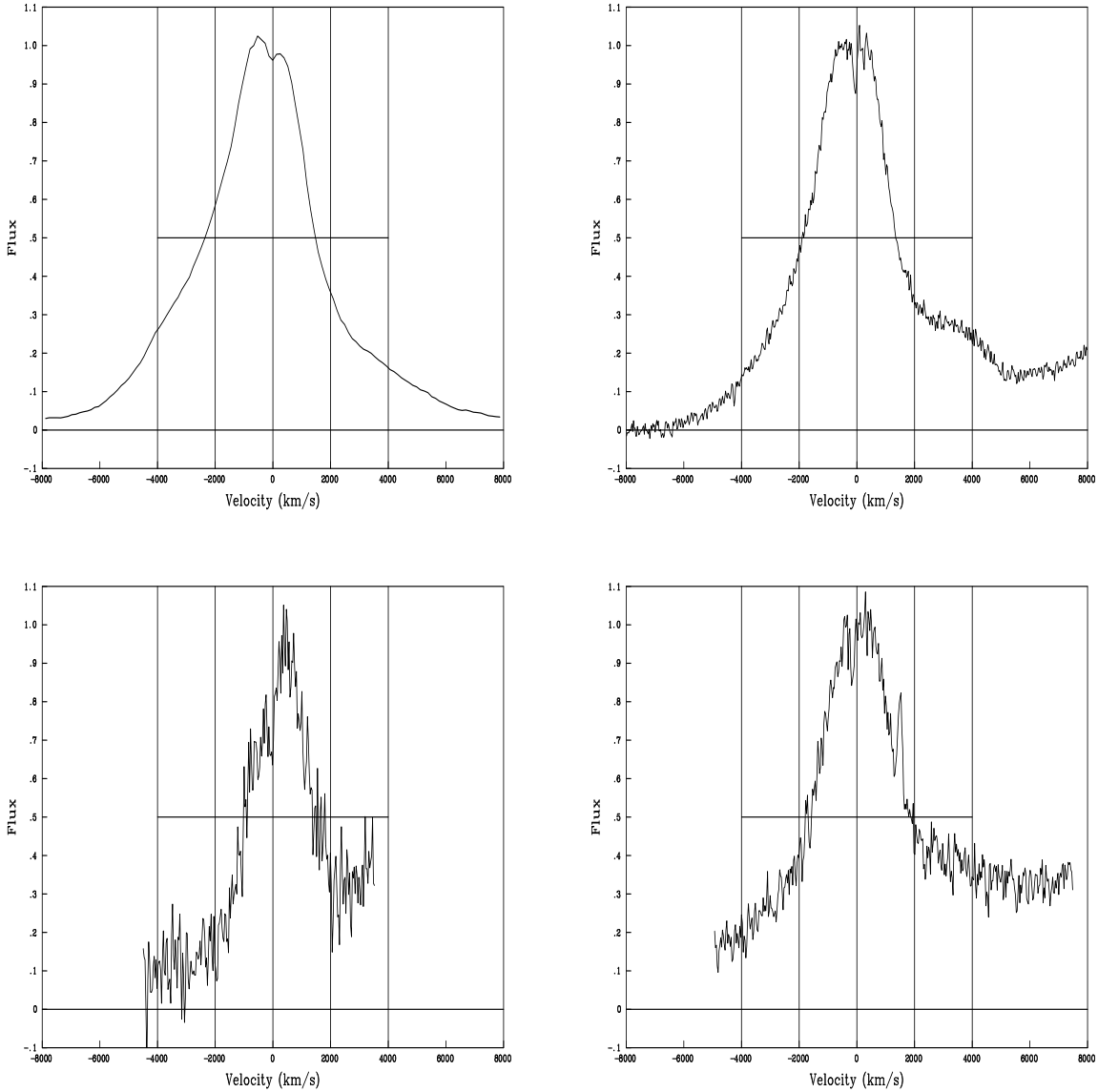


Figure 4. Velocity profile of the broad Balmer lines. The continuum has been subtracted and the top of the lines has been normalized to one. The vertical lines correspond to velocities equal to 0, ± 2000 and ± 4000 km s^{-1} . The horizontal line marks the point of half maximum. The lines are (from left to right and from top to bottom) $\text{H}\alpha$, $\text{H}\beta$, $\text{H}\gamma$ and $\text{H}\delta$.

high densities the following relationship applies (Osterbrock 1989):

$$\frac{I_{5959} + I_{5007}}{I_{4363}} \sim \frac{7.73 \times e^{\frac{32.29 \times 10^4}{T}}}{1 + 4.5 \times 10^{-4} \frac{N_e}{\sqrt{T}}}$$

The ratio of intensities in our case is 0.96. If we assume T to be on the range $10^5 - 10^7$ K, the density of the CSM is between 1×10^8 and $5 \times 10^7 \text{ cm}^{-3}$.

Note as well, that the presence of $[\text{N II}]$ 5755 Å and the absence of $[\text{N II}]$ 6583 Å and of $[\text{S II}]$ 6716, 6732 Å indicate that the latter are collisionally suppressed and therefore the CSM must have a high density.

4.2 Origin of the CSM

The origin of such a dense material around SN 1997eg is most probably related to a wind from the progenitor star. However, there are two possibilities to explain the velocity of expansion of the CSM and its high density.

The first, (proposed for SN 1997ab, Salamanca et al. 1998) is that this material is entirely due to a wind of the progenitor star shortly before it exploded as a supernova. The velocity and density of the CSM are those of the wind. This constrains the possible candidates that are able to explode as Type IIIn SN. From the analysis of the spectra we can deduce the physical conditions of this CSM, as well as the mass loss rate of the progenitor star. Following the same analysis as for SN 1997ab (Salamanca et al. 1998), we de-

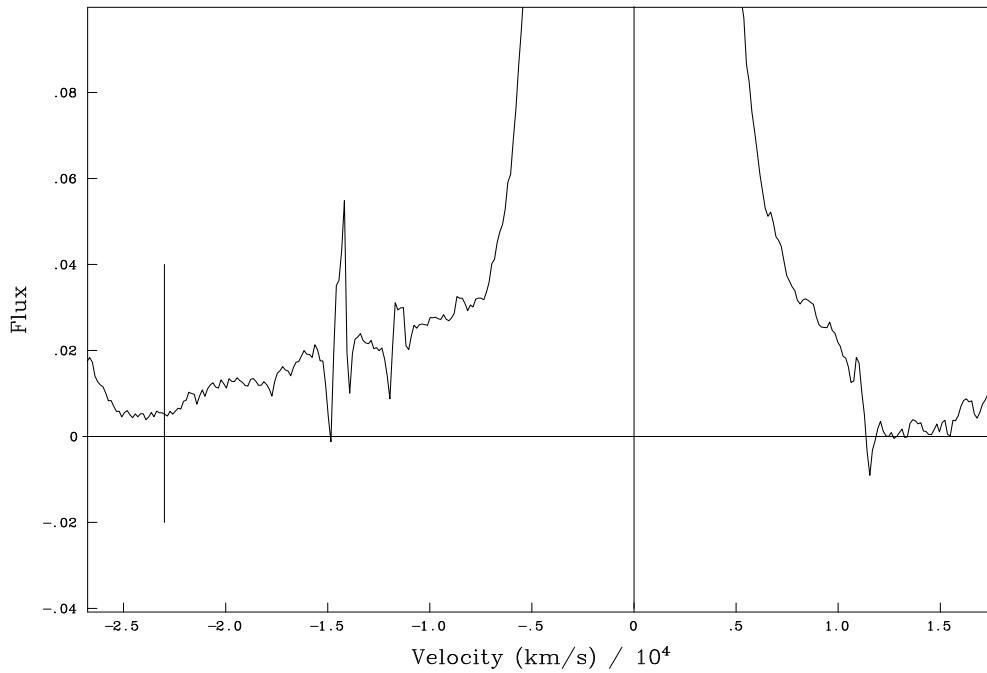


Figure 5. Velocity profile of the wings of the H α line. The continuum has been subtracted and the top of the line has been normalized to one. The vertical line marks the approximated end of the very extended wing, $\sim 23000 \text{ km s}^{-1}$.

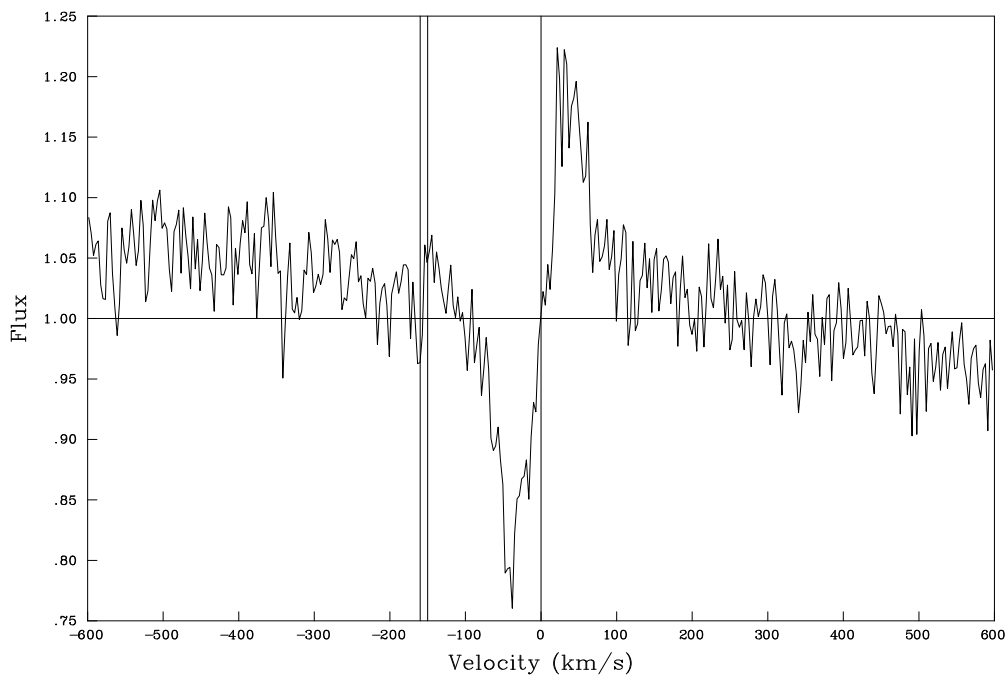


Figure 6. Velocity profile of the narrow P Cygni H α line. The top of the broad line has been normalized to one. The vertical lines marks the center of the P Cygni and the approximated blue end of the absorption $\sim 150 - 160 \text{ km s}^{-1}$.

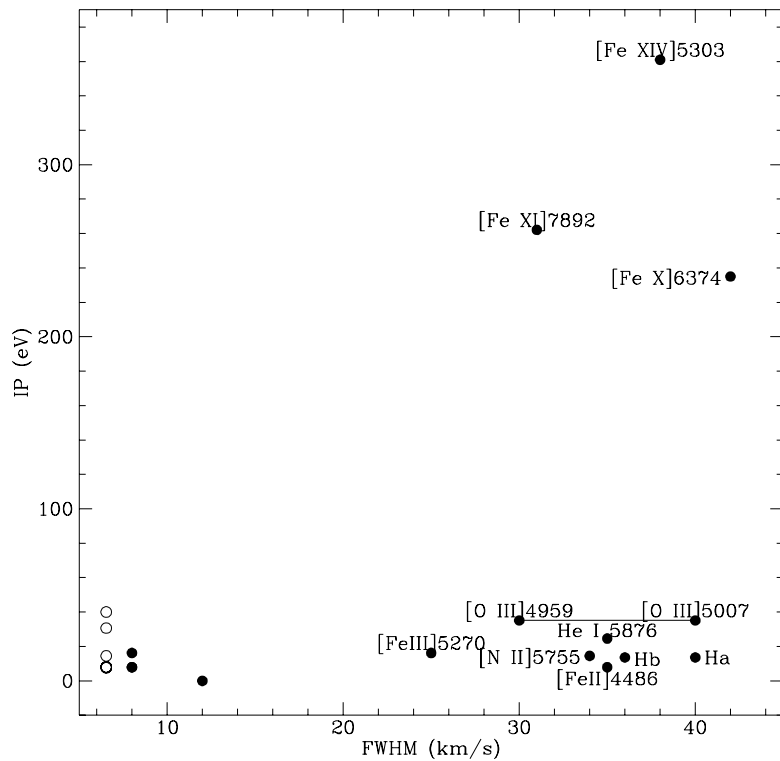


Figure 7. Ionization potential versus the FWHM of the narrow lines. Only those lines in the echelle data have been used. As well, those lines whose identification was not clear have been removed from the plot. The open circles at the bottom left correspond to those lines which were unresolved.

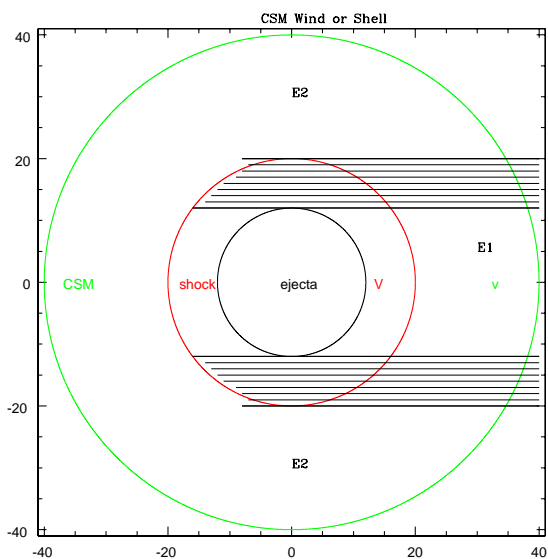


Figure 8. The different layers in both cases, CSW and CSSh. The observer is situated on the right side. The absorption would come from the shadowed area, where the projected velocities of the ejecta and the CSM are equal. This, seen from the front would form a narrow ring. The emission would come from the areas labeled E1 and E2.

duce that the mass loss rate of the progenitor star was $\dot{M} = 8.3 \times 10^{-3} M_{\odot} \text{ yr}^{-1}$, and that the radius of the shock is of the order of few times 10^{15} cm. We must draw the attention to the fact that in this case the density profile of the CSM declines as r^{-2} .

Another possibility is that the expansion of the CSM is the direct consequence of the supernova explosion, and more precisely, of the pre-ionisation of the CSM by the leading shock. In this case the CSM is created through a “normal” wind in a high pressure interstellar medium (ISM). If the progenitor star was in a high pressure ISM, then the wind will expand until it reaches the so-called “stagnation point”, where it will stop expanding and will accumulate creating a very dense shell of constant density. When the star explodes as a supernova, the ejecta first expands through the progenitor wind until it reaches the dense shell. At that moment, the phenomena of catastrophic cooling occurs and a luminous remnant is produced (see section 4). The flux produced at that moment will pre-ionize[‡] the CSM that will acquire a temperature of 10^{6-7} K and a thermal velocity $v_{th} \approx c_s$ where c_s is the velocity of the sound. Therefore, the pressure of the CSM gas will not longer be equal to the pressure of the ISM and it will start to expand with $v_{exp} \approx v_{th} \approx c_s$, until it reaches a new stagnation point. For the range of temperatures of the CSM ($\sim \text{few} \times 10^5$ to $\text{few} \times 10^6$ K) the velocity of the sound is ~ 55 to 170 km s^{-1} .

To distinguish both cases, we called the free expanding pre-SN wind “Circumstellar Wind” or CSW, and the second “Circumstellar Shell” or CSSh. Note however, that these are two *extreme* cases, and that a combination of both is not only possible, but probable. A very simple geometry of the different layers is illustrated on Fig. 8.

4.3 Comparison with previous models

We can compare the measured luminosities of the $H\alpha$ and $H\beta$ emission lines (broad and narrow) with the theoretical values obtained with the model of Terlevich et al. (1992, 1995). These values vary as a function of time, which is measured in units of the time at which the forward shock enters the radiative phase, t_{sg} . Assuming free-free cooling, t_{sg} is given by the expression (Shull 1980, Wheeler et al. 1980):

$$t_{sg} = 230 \left(\frac{E}{10^{51} \text{ erg}} \right)^{1/8} \left(\frac{n_{csm}}{10^7 \text{ cm}^{-3}} \right)^{-3/4} \text{ days} \quad (1)$$

where E is the initial kinetic energy of the supernova explosion and n_{csm} is the density of the circumstellar material.

The luminosities of the narrow Balmer lines also depend on the mass of the CSM. In Tab. 3 we give the values for $10 M_{\odot}$ and $20 M_{\odot}$. The density of the CSM is assumed constant and equal to 10^7 cm^{-3} .

If we assume that the density of the CSM is $\sim 1 \times 10^8 - 5 \times 10^7 \text{ cm}^{-3}$, then $t_{sg} \approx 41 - 69$ days (for $E = 1 \times 10^{51} \text{ erg}$). On the other hand, since the SN was not seen 4 months before the discovery, t_{sg} cannot be greater than ~ 120 days. These short values of t_{sg} imply that if the CSM is in a detached layer, it cannot be too far away from the SN. It

[‡] This is, prior to the ejecta -dense CSM collision.

means as well that the value of t/t_{sg} when SN 1997eg was observed was between 3 and 5. If we now compare the values given in Table 3 for t/t_{sg} with the measured values of the luminosities given in section 4.1, we conclude that the mass of the CSM must be around $10 M_{\odot}$. However, these values are only indicative, and a more detailed modelization of SN 1997eg remains to be done.

4.4 Profile of the Narrow P Cygni

In both cases (CSW or CSSh) the dense material in front of the shock will produce a P Cygni profile. The narrow absorption line is produced in a narrow ring where the projected velocities of the shock and CSM are equal. Moreover, it will be displaced to the blue, because we only see the gas that is coming towards us. And it will be a narrow profile because the range of velocities observed is small (see Fig. 6). However, depending on the case, CSW or CSSh, the details of it will be different. The evolution of it will be as well different. In the CSW case, the velocity of the wind should be already $\sim 160 \text{ km s}^{-1}$ when the supernova exploded. Therefore, the P Cygni profile should stay pretty much constant. In the CSSh case, the initial velocity of the CSM is zero, and it is accelerated to 160 km s^{-1} as the rarefaction wave crosses it. This should be reflected in an evolution with time of the P Cygni profile.

The emission comes from two zones (E1 and E2 in Fig. 8). From the gas coming towards us, we will see a blue-shifted emission. Since the projected velocity will be larger, this feature will be more blue-shifted than the absorption line. If the gas moving away from us is not totally obscured, we may see another redshifted emission. From the zone denominated E2 we see gas coming to and from us, and thus the resultant profile will be centered at the rest frame. However, the blue side will be masked by the absorption.

Of course, depending on the relative width of the different layers or shells and of their optical depth, the resulting P Cygni profile will be different. A detailed study for the CSW case is to be found in Cid-Fernandes (1999). For the CSSh case, this needs to be done.

5 DISCUSSION: CIRCUMSTELLAR WIND OR CIRCUMSTELLAR SHELL?

After a certain time, when the rarefaction wave has crossed all the Circumstellar Material, both cases - CSW and CSSh - will be undistinguishable. A good observational test would be to monitor with high resolution spectroscopy the same Type IIIn supernova at different epochs, starting as close as possible to the explosion date. If the the P Cygni profile remains constant, then this will point to a CSW, otherwise to a CSSh. In other words, we need high *spectral and temporal* resolution spectra to be able to deduce which is the density profile of the CSM. Furthermore, the other narrow lines associated with the CSM should give us a good deal of information. Does the ratio of Oxygen lines [O III] 4363/5007 remains constant with time? Are other coronal lines appearing at a later epoch? Is there any evolution in their luminosities or ratios? If yes, is this evolution the same as in the continuum or as in the broad Balmer lines?

Besides, we must not forget that Type IIIn SN are not

Table 3. Luminosities of the Balmer broad ($H\alpha$ luminosity and Balmer decrement) and narrow (idem) emission lines, calculated with the canonical model of Terlevich et al. (1992, 1995). The density of the CSM is constant and equal to 10^7 cm^{-3} , and the initial energy of the supernova explosion is equal to $1 \times 10^{51} \text{ erg}$.

t/t _{sg}	H α Broad	Balmer dec		Balmer dec. N		
		20 M $_{\odot}$	10 M $_{\odot}$	20 M $_{\odot}$	10 M $_{\odot}$	
1	41.38	3.7	39.14	38.76	5.5	4.9
4	41.22	6.9	40.12	39.96	6.3	4.8
8	40.87	14.4	39.78	-	5.0	-
16	40.24	21.7	39.37	-	4.0	-

only very energetic in the visible, but as well in X-rays (Fabian & Terlevich 1996, Lewin, Zimmermann, Aschenbach 1995) or Radio (Van Dyk et al 1993). In order to have a global and complete picture, we should have multi-monitoring campaigns in the same way as is done with AGN (e.g. Peterson & Wandel 2000, Edelson et al. 2000, Nandra et al 1998). Only then we would have enough observational constraints for the theoretical models. In particular, we should be able to deduce observationally the physical parameters of the CSM. This is so important because such CSM gives us important clues about the progenitor star and its environment. In the CSW case, this wind must be extremely dense. Its existence gives us direct clues about the nature of the progenitor star. In the CSSh case, the wind could be a “normal” RSG wind, but the progenitor must be embedded into a very high pressure medium. In such case, the progenitor wind gives us information about the regions where the star has formed and lived.

If we assume the CSW case, from the values of \dot{M} and v_w inferred we can constrain possible candidates for progenitors. Let’s examine three of them, known to have important mass losses: O stars, Wolf-Rayet stars and Luminous Blue Variables (also called S Dor variables).

O-stars have winds with $\dot{M} \sim 10^{-5} M_{\odot} \text{ yr}^{-1}$ and velocities of typically 10 km s^{-1} . Recent calculation by Panagia & Bono (2000) show that massive stars can have higher mass loss rates, up to $\sim 10^{-3} M_{\odot} \text{ yr}^{-1}$ and with velocities up to 50 km s^{-1} . However, this is out of the range of values measured for SN 1997ab or 1997eg.

Wolf-Rayet stars have much faster and massive winds: the velocity of their winds is of the order of $\text{few} \times 10^3 \text{ km s}^{-1}$ and the mass loss rates are $\sim 2 \times 10^{-5} M_{\odot} \text{ yr}^{-1}$ (Abbott & Conti 1987). Again, those numbers are different for what we find in SN 1997eg. However, they are more close to the values derived for less luminous Type II_n supernovae (see section 5.1).

Luminous Blue Variables stars (LBV) (see Humphreys & Davidson 1994 for a review) can experience very high mass losses in a very short time, during giant eruptions. The maximum mass lost rates deduced for LBV are in the order of $\dot{M} \sim 10^{-3} - 10^{-4} M_{\odot} \text{ yr}^{-1}$. For some cases, (e.g. η Carinae) the mass loss rate could reach values up to $\sim 10^{-1} M_{\odot} \text{ yr}^{-1}$ (Davidson 1989). This “super-wind” has a velocity within the values measured for the CSM $\sim 40 \text{ km s}^{-1}$ up to 700 km s^{-1} . The density of the nebula created by this wind is also in the range of densities measured for the material around Typw II_n SN : $n_e \sim 10^3$ to 10^7 cm^{-3} (Stahl 1989).

Obviously, the issue of the nature of the progenitors of Type II_n deserves more thorough investigation, but the possibility that they are post LBV stars opens an interesting question.

In we place ourselves in the CSSh case, then this means that the progenitor star was inside a very high pressure ambient medium. Where can we find such a medium? The most obvious answer is in star forming regions, where the wind of many massive stars and supernova explosions can create such high ambient pressure medium. One may ask then, why we do not see more of this Type II_n supernovae on Starburst galaxies? The hypothesis, proposed by Terlevich et al. (1992, 1995), is that we *do see* them, and we call them Active Galactic Nuclei (AGN).

5.1 Other cases of narrow P Cygni profiles

It is becoming clear that the narrow P Cygni of SN 1997eg is not an exception, but rather a common feature of Type II_n supernovae, at least in the initial stages of their evolution. The cases known until now are SN 1995G (Filippenko & Schlegel 1995, Turatto private communication), SN 1997ab (Salamanca et al. 1998) and SN1998S (Fassia et al 2001). The expansion velocity of the CSM deduced for SN 1997ab was $v_w \sim 90 \text{ km s}^{-1}$ and for SN 1998S, $v_w \sim 45 \text{ km s}^{-1}$. These values seem to indicate that there is a range in the velocities of the dense CSM around Type II_n Supernovae.

Moreover, there are less luminous Type II_n supernovae (classified as Type II_d by Benetti et al. 1998), which also have P Cygni profiles atop the broad emission lines. The difference with the more luminous SN II_n are that the P Cygni lines are somewhat broader (of about 1000 km s^{-1}) and that the broad emission lines are narrower, and less luminous. This can be explained by a lower CSM density, $n \sim 10^5 \text{ cm}^{-3}$, and by a lower mass loss rate of the progenitor star, $\dot{M} \sim 10^{-4}$ (assuming the CSW hypothesis). A good example is SN 1994aj (Benetti et al. 1998).

Another example of detection of the dense CSM is SN 1978K (Chu et al. 1999).

6 CONCLUSIONS

There is strong observational evidence for the existence of a dense and hot CSM in Type II_n SN, particularly in SN 1997eg. Such dense environment was “necessary” from the theoretical point of view, because the physical explanation invokes the presence of radiative shocks, produced via

the interaction of the SN ejecta with dense material. Echelle spectrum of SN 1997eg shows a very narrow P Cygni line atop the broad emission on H α and H β . This feature seems to be common in Type II_n SN in their early stages, and points to either a massive and slow wind of the progenitor just prior to the explosion or to a wind in a high pressure medium, as its origin.

However, even though the data presented here answer many questions concerning such CSM, it opens even more, which can only be addressed with more data. Instead of concentrating in small details of SN II_n, long-term, multi-wavelength monitoring of such objects would be the right thing to do (e.g. Aretxaga et al. 1998) in a similar way as is done for AGN (see for example Peterson & Wandel 2000).

ACKNOWLEDGEMENTS

I.S is deeply obliged to Maureen van der Berg for her help in calibrating the echelle spectra and to Dr. Arnout van Genderen for his useful comments on an earlier draft of this paper. We are as well thankful to the anonymous referee for his/her comments which have improved the clarity of the paper.

This research has been supported by a Marie Curie Fellowship of the European Community programme “Training and Mobility of Researches” awarded to I. Salamanca (proposal Nr. ERB4001GT974289).

This project has been supported by the European Commission through the Activity “Access to Large-Scale Facilities” within the Program “Training and Mobility of Researches”, awarded to the Instituto de Astrofísica de Canarias to fund European Astronomers’ access to its Roque de los Muchachos and Teide Observatories (European Northern Observatory), in the Canary Islands.

REFERENCES

- Abbott D.C., Conti P.S., 1987, *ARA&A*, 25, 113
- Aretxaga I., Benetti S., Terlevich R.J., Fabian A.C., Cappellaro E., Turatto M., della Valle M., 1998, *MNRAS*, 309, 343
- Benetti S., Cappellaro E., Danzinger I.J., Turatto M., Patat F., Della Valle M., 1998, *MNRAS*, 294, 448
- Chevalier R.A., Fransson C. 1994, *ApJ*, 420, 268
- Chu Y.-H., Caulet A., Montes M.J., Panagia N., van Dyk S. D., Weiler K. W., 1999, *ApJ*, 512, L51
- Chugai N.N., 1991, *MNRAS*, 250, 513
- Cid-Fernandes R., 1999, *MNRAS*, 305, 602
- Davidson K., 1989, in Davidson K., Moffat A.F.J., Lamers H.J.G.L.M., eds., *Physics of Luminous Blue Variables*, Kluwer Academic Publ., p. 101
- Edelson R., Koratkar A., Nandra K. et al., 2000, *ApJ*, 534, 180
- Fabian A.C., Terlevich R.J., 1996, *MNRAS*, 280, L5
- Fassia A., Meikle W.P.S., Chugai N. et al., 2001, *MNRAS*, 325, 907
- Filippenko A.V., Barth A.J., 1997, IAU Circular no. 6794
- Filippenko A.V., Schlegel D., 1995, IAU Circular no. 6139
- Ho L.C., Filippenko A.V., Sargent W.L.W., 1997, *ApJS*, 112, 315
- Humphreys R.M., Davidson K., 1994, *PASP*, 106, 1025
- Lacey C.K., Weiler K.W., 1998, IAU Circular no. 7068
- Lewin W.H.G., Zimmermann H.-U., Aschenbach B., 1995, IAU Circ no. 6445
- Meikle P., Geballe T., 1998, *UKIRT Newsletter* vol 3
- Nandra K., Clavel J., Edelson R.A., George I.M., Malkan M.A., Mushotzky R.F., Peterson B.M., Turner T.J., 1998 *ApJ*, 505, 594
- Nakano S., Masakatsu A., 1997, IAU Circular no. 6790
- Osterbrock D.E., 1989, *Astrophysics of Gaseous Nebulae and Active Galactic Nuclei*. Mill Valley, CA, University Science Books
- Panagia N., Bono G., 2000, in Livio M., Panagia N., Sahu K., eds., *STScI May Symposium, “The Largest Explosions since the Big-Bang: Supernovae and Gamma Ray Bursts”*, CUP-Cambridge, in press.
- Peterson B.M., Wandel A., 2000 *ApJ*, 540, L13
- Salamanca I., Cid-Fernandes R., Tenorio-Tagle G., Telles E., Terlevich R.J., Muñoz-Tuñon C., 1998, *MNRAS*, 300, L17
- Shull M., 1980, *ApJ*, 237, 769
- Stahl O., 1989, in Davidson K., Moffat A.F.J., Lamers H.J.G.L.M. eds., *Physics of Luminous Blue Variables*. Kluwer Academic Publ., p. 149
- Terlevich R.J. Tenorio-Tagle G., Franco J., Melnick J., 1992, *MNRAS*, 255, 713
- Terlevich R.J., Tenorio-Tagle G., Rozyczka M., Franco J., Melnick J., 1995, *MNRAS*, 272, 198
- Van Dyk S.D., Weiler K.W., Sramek R.A., Panagia, N., 1993 *ApJ*, 419, L69
- Wheeler J.C., Mazurek T.J., Sivaramakrishnan A., 1980, *ApJ*, 237, 781

This paper has been produced using the Royal Astronomical Society/Blackwell Science L^AT_EX style file.